Three-Dimensional Electrical Control of the Excitonic Fine Structure for a Quantum Dot in a Cavity

H. Ollivier,[1] P. Priya,[1] A. Harouri,[1] I. Sagnes,[1] A. Lemaître,[1] O. Krebs,[1] L. Lanco,[1,2] N. D. Lanzillotti-Kimura,[1] M. Esmann,[1,*,‡] and P. Senellart[1,†]

[1]*Université Paris-Saclay, CNRS, Centre de Nanosciences et de Nanotechnologies (C2N), 10 Boulevard Thomas Gobert, 91120 Palaiseau, France*

[2]*University Paris Cité, Centre de Nanosciences et de Nanotechnologies (C2N), 91120 Palaiseau, France*

(Received 1 December 2021; accepted 27 May 2022; published 25 July 2022)

The excitonic fine structure plays a key role for the quantum light generated by semiconductor quantum dots, both for entangled photon pairs and single photons. Controlling the excitonic fine structure has been demonstrated using electric, magnetic, or strain fields, but not for quantum dots in optical cavities, a key requirement to obtain high source efficiency and near-unity photon indistinguishability. Here, we demonstrate the control of the fine structure splitting for quantum dots embedded in micropillar cavities. We propose and implement a scheme based on remote electrical contacts connected to the pillar cavity through narrow ridges. Numerical simulations show that such a geometry allows for a three-dimensional control of the electrical field. We experimentally demonstrate tuning and reproducible canceling of the fine structure, a crucial step for the reproducibility of quantum light source technology.

DOI: 10.1103/PhysRevLett.129.057401

Semiconductor quantum dots (QDs) have emerged as excellent emitters of single photons [1] and entangled photon pairs [2,3] with exciting prospects for both optical quantum networks and processors. The neutral exciton state in an epitaxially grown QD exhibits a fine structure splitting (FSS) arising from a reduced symmetry of the nanostructure as well as valence band mixing [see Fig. 1(b)] [4,5]. Canceling this FSS has long been identified as a key requirement for the on-demand generation of polarization-entangled photon pairs via the radiative biexciton-exciton cascade [6,7]. Similarly, near-zero FSS was shown to enable high fidelity initialization of long-lived quantum dot hole spin qubits [8]. Conversely, it was very recently shown that the brightness of an exciton based single-photon source under resonant pumping could be optimized for an optimal finite FSS value [9]. A large variety of techniques are thus explored to control the FSS. Material growth and processing are tailored to reduce the average FSS—for instance, growing small QDs [10], performing postgrowth annealing [11], or using droplet epitaxy [12]. Fine-tuning of the residual FSS is explored through the application of both magnetic and electric fields [10,13,14] as well as strain [15,16]. However, the control of a single degree of freedom only leads to zero FSS if the applied field points along the major axis of QD asymmetry [17–19]. To universally eliminate the FSS, it was theoretically shown that two independent and nonparallel external controls are needed [20], e.g., biaxial strain or two vector components of an applied electromagnetic field. Adding a third control further allows independent tuning of the FSS and the average exciton transition energy [21].

Over the years, the toolbox for controlling the FSS has become diverse and efficient, leading to record entanglement fidelity for entangled photon pairs [22]. However, such control has not yet been achieved for QDs inserted in optical cavities, a crucial step to ensure high collection efficiency of the single and entangled photons [23–25],

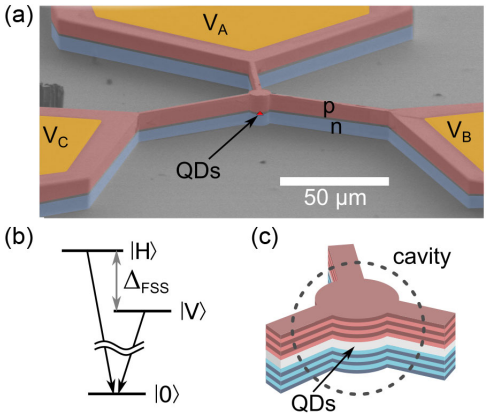

FIG. 1. (a) SEM image of a 10 μm diameter micropillar cavity with QDs embedded at its center. Ridges connect the pillar to three electrical contacts defined via gold pads. The image has been artificially colored to evidence the different components of the structure. (b) Schematic of the exciton energy levels. (c) Schematic enlargement of the pillar structure highlighting the top and bottom cavity mirrors defining the cavity in the vertical direction. The QD layer is vertically centered in the cavity.

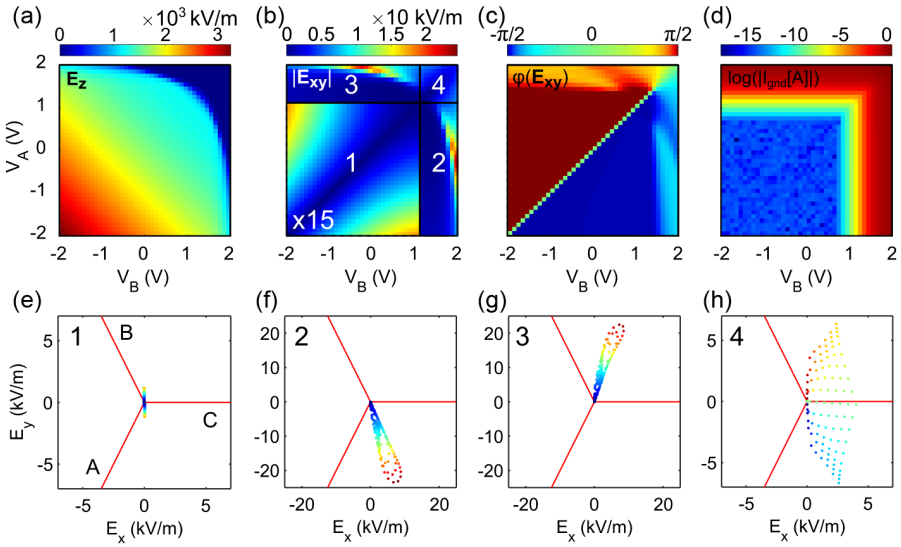

FIG. 2. FEM simulation as a function of V_A and V_B (unconnected diode C). (a)–(c) Calculated electric field E_z, amplitude $|E_{xy}|$, and angle $\varphi(E_{xy})$ of the in-plane field. $\varphi = 0$ is the direction along ridge C. (d) Calculated net current flowing through the device. Four regions are defined in (b): (1) nonpassing, (2),(3) one diode passing, and (4) two-diode passing [see panel (d)]. $|E_{xy}|$ in region (1) was multiplied by 15 for better visualization. (e)–(h) Distribution of in-plane electric field for regions (1)–(4). Red lines mark the orientation of ridges A–C. Each point in (e)–(h) corresponds to a value pair (V_A, V_B) in steps of 0.1 V. The color of each point in (e)–(g) [respectively (h)] is the same as for the corresponding point in panel (b) [respectively (c)].

and for reaching near-unity photon indistinguishability [23,24,26].

Here, we propose a structure that allows controlling the excitonic FSS for quantum dots inserted in monolithic micropillar cavities. We define three independent control knobs by remotely applying three electric potentials on large p-i-n diodes that are connected to the pillar cavity through narrow ridges. The vertical p-i-n doping profile extends over the full device. Finite element simulations are conducted to monitor both the stationary electric field and current in the structure for various bias situations, evidencing a control of the electric field at the position of the QD in all three directions of space. We experimentally explore this approach and demonstrate both a control of the FSS amplitude and of the orientation of the exciton transition dipoles. We find that various combinations of applied voltages reduce the FSS close to or below the radiative linewidth. Furthermore, similar values of FSS can be obtained for different excitonic wavelengths.

The structure proposed to control the excitonic FSS for a QD in a cavity is illustrated in Fig. 1(a). We start from a planar GaAs/AlGaAs microcavity grown on a GaAs substrate. For the sample under investigation, the bottom (top) distributed Bragg reflector (DBR) consists of 34 (16) pairs of $\lambda/4$-thick GaAs/AlGaAs layers. The DBRs surround a λ-thick GaAs cavity spacer with a layer of annealed InGaAs QDs in its center. Vertically, the multilayer structure defines a p-i-n junction with p(n) doping for the top (bottom) mirror and an intrinsic region within the cavity spacer embedding the QDs. Laterally, the planar structure is etched to define circular pillar cavities with 10 μm diameters that are connected through three 3 μm wide, 50 μm long ridges to large mesas where titanium-gold pads are defined for electrical connection. Each pad can be connected to an independent voltage source with the gold-coated back of the substrate defining a common ground potential. By applying various values for the three biases labeled V_A, V_B, and V_C, one can control the amplitude and direction of the electric field at the center of the pillar cavity in the three directions of space.

To evidence such a possibility, we first performed a finite elements method (FEM) study (COMSOL Multiphysics). For computational efficiency, we replaced the vertical DBR layer structure by a single GaAs slab with a vertical p-i-n doping profile. Such a simplification allows for a qualitative understanding of the physics at play disregarding the complex modulation doping structure that one needs to implement in the DBR structure. Figures 2(a)–2(c) display the calculated electric field along z, E_z, as well as the amplitude $|E_{xy}|$ and in-plane angle φ of the in-plane electric field at the center of the micropillar cavity. We applied two electric potentials V_A and V_B, whereas V_C was not fixed by an external potential. $\varphi = 0$ corresponds to the direction along ridge C. Along the vertical direction, the calculated electric field E_z presents a large amplitude for negative values of V_A and V_B, and progressively decreases when going to the passing regime for both diodes A and B. The in-plane electric field components, on the other hand, show a more subtle behavior and four regimes can be identified as indicated in the four areas labeled 1 through 4 in Fig. 2(b). They essentially correspond to the regimes of nonpassing and passing p-i-n junctions for each of the two

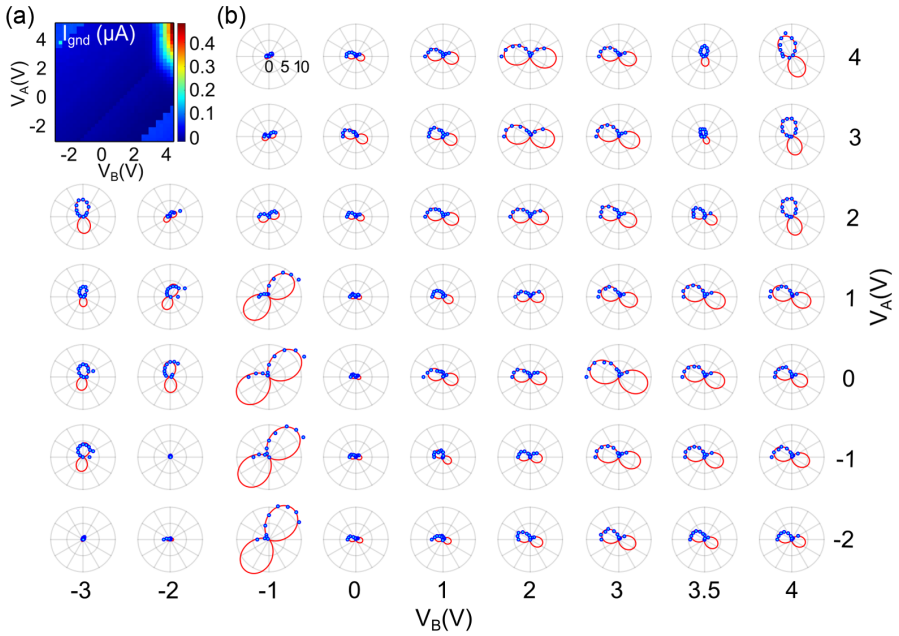

FIG. 3. (a) Measured net current flowing through the p-i-n junction as a function of V_A and V_B. (b) Polar plots of the exciton energy shift in QD1 as a function of the linear polarization angle of detection (blue circles) for various value pairs of V_A and V_B together with fits to a sine function (solid red lines). The scale for the radial direction is given in the top-left polar plot in units of μeV. The FSS reduces down to 0.4 ± 0.20 μeV for $V_B = -2$ V and $V_A = -1$ V, a value well below the radiative linewidth of typically 1 μeV for QDs in bulk.

electric potentials as evidenced by Fig. 2(d) presenting the total current flowing through the device (in logarithmic scale).

Figures 2(e)–2(h) present the in-plane electric field components in polar plots for each regime. Each point corresponds to a value of (V_A, V_B) by steps of 0.1 V and its color provides some correspondence between Figs. 2(e)–2(h) and 2(b), 2(c) (see figure caption). For area 1 [Fig. 2(e)], the amplitude of the in-plane field amplitude depends mostly on the applied voltage difference $|V_A - V_B|$ but its direction remains normal to the unconnected ridge C ($\varphi = \pm\pi/2$): the current flows along the p-doped upper DBR with an in-plane field parallel to it, dictated by the Ohmic resistivity of the p-doped material (see Supplemental Material [27], Fig. S2). Note that in the same area, E_z depends mainly on the mean of the applied potentials $\frac{1}{2}(V_A + V_B)$.

The direction of the in-plane electric field is modified when the junctions are in the passing regime. For the regime in which only diode A (B) is passing, corresponding to Figs. 2(f) and 2(e), the field mostly points in the direction away from diode A (B), yet with a noticeable steering effect resulting from the second applied voltage presenting a current drain on the top surface. Finally, when both diodes are passing [Fig. 2(h), corresponding to area 4 in Fig. 2(b)], the angle φ of the in-plane electric field covers a range of almost π. Effectively, we generate two independent nonparallel current components that are both drained to the common ground on the back side of the p-i-n junction.

There are thus at least two ways to generate in-plane electric fields with directional control at the center of the cavity. First, for a nonpassing p-i-n junction, using the third control knob V_C (in addition to V_A and V_B) would allow one to control the field amplitude in the three directions normal to each one of the ridges as it was the case for the direction normal to ridge C with only one pair of voltages (V_A and V_B) in Fig. 2(e). Second, for large forward bias, two electric potentials suffice to control both orientation and magnitude of the field.

The link between the observed in-plane electric field behavior and current flows is shown in Fig. S2 in the Supplemental Material [27]. In all regimes, except for area 4, the current and electric field are roughly parallel to each other. For area 4, two nonparallel current components are created that are both drained through the p-i-n junction in the passing regime. We emphasize, however, that the absolute value of the calculated current is largely overestimated numerically because of the strongly simplified doping structure considered in the z direction, as experimentally evidenced hereafter.

We tested this scheme experimentally on 10 μm diameter pillar cavities that do not show discrete optical modes, hence avoiding any cavity birefringence effect that could perturb the polarization analysis [28]. We perform polarization-resolved microphotoluminescence (μPL) studies at 4 K, under quasiresonant (p-shell) continuous-wave excitation [29]. We studied two QDs (QD1 and QD2) inserted into two distinct cavities. Figure 3 shows the experimental data obtained for QD1 and Fig. 4 for QD2. Complementary measurements for both QDs are shown in the Supplemental Material [27]. Figure 3(a) presents the measured sum of

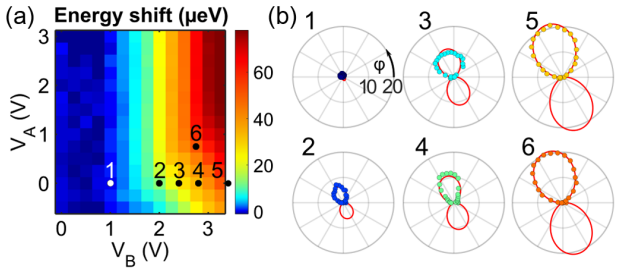

FIG. 4. Measurements for QD2. (a) Energy shift of the averaged exciton transition as a function of V_A and V_B relative to its energy at $V_A = V_B = 0$. (b) Polar plots of the exciton energy shift as a function of the linear polarization angle of detection (circles) for the 6 points indicated in (a). The color of the points corresponds to the energy shift color scale shown in (a).

currents flowing through the connections to the two independent voltage sources. This sum corresponds to the portion of the current that flows through the p-i-n junction, since the horizontal current flowing on top of the device cancels out in this calculation. Figure 3(a) allows one to identify the various regimes for the FSS control and evidences maximal current in the μA range, orders of magnitude lower than predicted by our simplified numerical simulations. The passing regime is obtained for $V_A \geq 2$ V and $V_B \geq 4$ V. This asymmetry, which is not accounted for in our numerical simulations, can be due to imperfections of the 1D ridges exhibiting different Ohmic resistances; see Fig. S6 in the Supplemental Material [27].

We obtain the FSS by measuring the exciton peak energy that undergoes a sinusoidal shift of amplitude Δ_{FSS} as a function of the angle θ of the detected linear polarization (see Fig. S1, Supplemental Material [27]). In Fig. 3(b), polar plots of this shift are reported for different voltages V_B and V_A. For each voltage, the angular dependence is fitted by the function $\Delta_{\mathrm{FSS}}(\cos[2(\theta - \theta_0)] + 1)/2$ where θ_0 refers to the polarization angle of the high energy exciton line. Strong variations of both the amplitude of the FSS (up to $\sim$20 μeV) together with a rotation of the exciton eigenaxes are observed depending on the applied voltages. The characteristic signature of a cancellation of the FSS, where the eigenaxes of the high and low energy exciton lines are exchanged when (ideally) crossing the zero FSS point [19,20], is observed for both the passing regime (V_A around 3 V and V_B around 3.5 V) and the nonpassing regime ($V_A < 0$ V and $V_B < 0$ V). We note that a reduction of the FSS down to 0.4 ± 0.20 μeV is observed for $V_B = -2$ V and $V_A = -1$ V, a value well below the radiative linewidth of typically 1 μeV for QDs in bulk [30]. Finally, we note that the FSS varies nonmonotonously, showing various local minima. Such an observation is not directly explained by the electrical field, which, according to our numerical simulations, should evolve monotonously. This rather reveals the complex dependence of the FSS on the electric field, as already reported in Ref. [14] for an electric field applied in plane.

Similar results for QD2 are reported in Fig. 4(b) for a smaller dataset evidencing an FSS down to 1.3 ± 0.7 μeV for point $V_A = 0$ V and $V_B = 1$ V, again below the radiative linewidth within error bars. Figure S4 in the Supplemental Material [27] shows an extended dataset, evidencing a nonmonotonous variation of the FSS very similar to the one observed for QD1. Figure 4(a) presents the average exciton energy shift for QD2 due to the quantum confined Stark effect as a function of both applied voltages. It demonstrates an energy shift within a range of around 80 μeV. This behavior, also observed for QD1 (see Fig. S3, Supplemental Material [27]) is of particular interest to reduce or modify the FSS for different central exciton energies. This possibility is evidenced in Fig. 4(b), where similar FSS values are obtained at different exciton energy for voltage combinations 3 and 4 as well as for 5 and 6, as indicated by the color of the measured points corresponding to the energy shift scale of Fig. 4(a).

Finally, we emphasize that the present method relies on a vertical doping structure and remote contact geometry very similar to the one already used with one contact only to obtain highly indistinguishable photons for QDs deterministically positioned in micropillar cavities [9,24]. It should thus allow high photon indistinguishability when combined with a resonant excitation scheme. Note that the nonresonant excitation was needed here to collect all polarization directions but would reduce indistinguishability because of charge noise (see Fig. S5, Supplemental Material [27]) and time jitter.

In conclusion, we have proposed a new scheme to control the exciton fine structure of a QD inside a cavity. We demonstrated a tuning of the FSS in the 10–20 μeV range [21,31], which is shown to be sufficient to cancel the FSS of annealed InGaAs QDs. We also reported an 80 μeV exciton energy tuning range—a value that is sufficient to tune the QD exciton into resonance with the pillar cavity mode when combined with the *in situ* lithography technique [32], a powerful technique to obtain bright sources of single or entangled photon pairs [24,25]. Several parameters can be explored to increase the amplitude of the electric field variation: length and width of the connecting ridges, vertical doping structures, etc. Our Letter thus opens the path toward the fabrication of bright sources of single photons and entangled photon pairs, with control of both the QD-cavity detuning and the excitonic fine structure.

This work was partially supported by the H2020-FET OPEN project no. 899544—PHOQUSING, the French RENATECH network, and the European Research Council Starting Grant No. 715939, Nanophennec. H. O. acknowledges support from the Paris Ile-de-France Région in the framework of DIM SIRTEQ. M. E. acknowledges funding by the Deutsche Forschungsgemeinschaft (DFG, German Research Foundation) Project 401390650, and by the University of Oldenburg through a Carl von Ossietzky Young Researchers fellowship.

*Corresponding author.
m.esmann@uni-oldenburg.de
†Corresponding author.
pascale.senellart-mardon@c2n.upsaclay.fr
‡Present address: Institute of Physics, Carl von Ossietzky University, 26129 Oldenburg, Germany.

[1] P. Senellart, G. Solomon, and A. White, Nat. Nanotechnol. **12**, 1026 (2017).
[2] C. Schimpf, M. Reindl, F. Basso Basset, K. D. Jöns, R. Trotta, and A. Rastelli, Appl. Phys. Lett. **118**, 100502 (2021).
[3] K. D. Jöns, L. Schweickert, M. A. M. Versteegh, D. Dalacu, P. J. Poole, A. Gulinatti, A. Giudice, V. Zwiller, and M. E. Reimer, Sci. Rep. **7**, 1700 (2017).
[4] M. Bayer, G. Ortner, O. Stern, A. Kuther, A. A. Gorbunov, A. Forchel, P. Hawrylak, S. Fafard, K. Hinzer, T. L. Reinecke, S. N. Walck, J. P. Reithmaier, F. Klopf, and F. Schäfer, Phys. Rev. B **65**, 195315 (2002).
[5] Y. Léger, L. Besombes, L. Maingault, and H. Mariette, Phys. Rev. B **76**, 045331 (2007).
[6] O. Benson, C. Santori, M. Pelton, and Y. Yamamoto, Phys. Rev. Lett. **84**, 2513 (2000).
[7] J. Liu, R. Su, Y. Wei, B. Yao, S. F. C. d. Silva, Y. Yu, J. Iles-Smith, K. Srinivasan, A. Rastelli, J. Li, and X. Wang, Nat. Nanotechnol. **14**, 586 (2019).
[8] A. J. Brash, L. M. P. P. Martins, F. Liu, J. H. Quilter, A. J. Ramsay, M. S. Skolnick, and A. M. Fox, Phys. Rev. B **92**, 121301 (2015).
[9] H. Ollivier, I. Maillette de Buy Wenniger, S. Thomas, S. C. Wein, A. Harouri, G. Coppola, P. Hilaire, C. Millet, A. Lemaitre, I. Sagnes, O. Krebs, L. Lanco, J. C. Loredo, C. Antón, N. Somaschi, and P. Senellart, ACS Photonics **7**, 1050 (2020).
[10] R. Stevenson, R. Young, P. Atkinson, K. Cooper, D. Ritchie, and A. Shields, Nature (London) **439**, 179 (2006).
[11] R. J. Young, R. M. Stevenson, A. J. Shields, P. Atkinson, K. Cooper, D. A. Ritchie, K. M. Groom, A. I. Tartakovskii, and M. S. Skolnick, Phys. Rev. B **72**, 113305 (2005).
[12] Y. Huo, A. Rastelli, and O. Schmidt, Appl. Phys. Lett. **102**, 152105 (2013).
[13] K. Kowalik, O. Krebs, A. Lemaitre, S. Laurent, P. Senellart, P. Voisin, and J. A. Gaj, Appl. Phys. Lett. **86**, 041907 (2005).
[14] B. Gerardot, S. Seidl, P. Dalgarno, R. Warburton, D. Granados, J. García, K. Kowalik-Seidl, O. Krebs, K. Karrai, A. Badolato, and P. Petroff, Appl. Phys. Lett. **90**, 041101 (2007).
[15] S. Seidl, M. Kroner, A. Högele, and K. Karrai, Appl. Phys. Lett. **88**, 203113 (2006).
[16] C. Kuklewicz, R. Malein, P. Petroff, and B. Gerardot, Nano Lett. **12**, 3761 (2012).
[17] M. Gong, W. Zhang, G.-C. Guo, and L. He, Phys. Rev. Lett. **106**, 227401 (2011).
[18] J. D. Plumhof, V. Krápek, F. Ding, K. D. Jöns, R. Hafenbrak, P. Klenovský, A. Herklotz, K. Dörr, P. Michler, A. Rastelli, and O. G. Schmidt, Phys. Rev. B **83**, 121302 (2011).
[19] A. Bennett, M. Pooley, R. Stevenson, M. Ward, R. Patel, A. Giroday, N. Sköld, I. Farrer, C. Nicoll, D. Ritchie, and A. Shields, Nat. Phys. **6**, 947 (2010).
[20] R. Trotta, E. Zallo, C. Ortix, P. Atkinson, J. D. Plumhof, J. van den Brink, A. Rastelli, and O. G. Schmidt, Phys. Rev. Lett. **109**, 147401 (2012).
[21] R. Trotta, J. Martín-Sánchez, I. Daruka, C. Ortix, and A. Rastelli, Phys. Rev. Lett. **114**, 150502 (2015).
[22] D. Huber, M. Reindl, S. F. Covre da Silva, C. Schimpf, J. Martín-Sánchez, H. Huang, G. Piredda, J. Edlinger, A. Rastelli, and R. Trotta, Phys. Rev. Lett. **121**, 033902 (2018).
[23] H. Wang, Z.-C. Duan, Y.-H. Li, S. Chen, J.-P. Li, Y.-M. He, M.-C. Chen, Y. He, X. Ding, C.-Z. Peng, C. Schneider, M. Kamp, S. Höfling, C.-Y. Lu, and J.-W. Pan, Phys. Rev. Lett. **116**, 213601 (2016).
[24] N. Somaschi, V. Giesz, L. De Santis, J. C. Loredo, M. P. Almeida, G. Hornecker, S. L. Portalupi, T. Grange, C. Antón, J. Demory, C. Gómez, I. Sagnes, N. D. Lanzillotti-Kimura, A. Lemaítre, A. Auffeves, A. G. White, L. Lanco, and P. Senellart, Nat. Photonics **10**, 340 (2016).
[25] A. Dousse, J. Suffczyński, A. Beveratos, O. Krebs, A. Lemaitre, I. Sagnes, J. Bloch, P. Voisin, and P. Senellart, Nature (London) **466**, 217 (2010).
[26] N. Tomm, A. Javadi, N. O. Antoniadis, D. Najer, M. C. Lobl, A. R. Korsch, R. Schott, S. R. Valentin, A. D. Wieck, A. Ludwig, and R. J. Warburton, Nat. Nanotechnol. **16**, 399–403 (2021).
[27] See Supplemental Material at http://link.aps.org/supplemental/10.1103/PhysRevLett.129.057401 for additional experimental data and numerical simulations.
[28] M. Moczała, Ł. Dusanowski, S. Gerhardt, Y. He, M. Reindl, A. Rastelli, R. Trotta, N. Gregersen, S. Höfling, and C. Schneider, ACS Photonics **6**, 2025 (2019).
[29] O. Gazzano, S. Michaelis de Vasconcellos, C. Arnold, A. Nowak, E. Galopin, I. Sagnes, L. Lanco, A. Lemaître, and P. Senellart, Nat. Commun. **4**, 1425 (2013).
[30] A. V. Kuhlmann, J. H. Prechtel, J. Houel, A. Ludwig, D. Reuter, A. D. Wieck, and R. J. Warburton, Nat. Commun. **6**, 8204 (2015).
[31] R. Trotta, J. Wildmann, E. Zallo, O. Schmidt, and A. Rastelli, Nano Lett. **14**, 3439 (2014).
[32] A. Dousse, L. Lanco, J. Suffczynski, E. Semenova, A. Miard, A. Lemaitre, I. Sagnes, C. Roblin, J. Bloch, and P. Senellart, Phys. Rev. Lett. **101**, 267404 (2008).